

Unclassified

9 JUN 1980 SECURITY CLASSIFICATION OF THIS PAGE (When Data Entered)

① LEVEL II

REPORT DOCUMENTATION PAGE		READ INSTRUCTIONS BEFORE COMPLETING FORM
1. REPORT NUMBER	2. GOVT ACCESSION NO.	3. RECIPIENT'S CATALOG NUMBER
4. TITLE (and Subtitle) STRUCTURE AND PROPERTIES OF RAPIDLY SOLIDIFIED 2000 SERIES Al-Li ALLOYS		5. TYPE OF REPORT & PERIOD COVERED Technical Report
7. AUTHOR(s) N. J. Grant, S. Kang W. Wang		6. PERFORMING ORG. REPORT NUMBER
9. PERFORMING ORGANIZATION NAME AND ADDRESS N. J. Grant Department of Materials Science & Engineering Massachusetts Institute of Technology - 8-305 Cambridge, MA 02139		8. CONTRACT OR GRANT NUMBER(s) N00014-78-C-0385 Amendment A00003 ARPA Order # 3558
11. CONTROLLING OFFICE NAME AND ADDRESS Advanced Research Projects Agency (ARPA) 1400 Wilson Boulevard Arlington, VA 22209		10. PROGRAM ELEMENT REPORT, TASK AREA & WORK UNIT NUMBERS 970400.1304 ARPA Order # 3558
14. MONITORING AGENCY NAME & ADDRESS (if different from Controlling Office) Office of Naval Research (ONR) Department of the Navy, 800 N. Quincy Street Arlington, VA 22217		12. REPORT DATE May 20, 1980
		13. NUMBER OF PAGES 21
		15. SECURITY CLASS (of this report) Unclassified
16. DISTRIBUTION STATEMENT (of this Report) Approved for public release -- distribution unlimited		15a. DECLASSIFICATION/DOWNGRADING SCHEDULE --
17. DISTRIBUTION STATEMENT (of the abstract entered in Block 20, if different from Report) --		
18. SUPPLEMENTARY NOTES Paper presented at the First International Conference on Aluminum-Lithium Alloys, Stone Mountain, Georgia, May 19-21, 1980 and also to be published as part of the proceedings of the above conference.		
19. KEY WORDS (Continue on reverse side if necessary and identify by block number) Rapid solidification Tension properties Aluminum alloys, Al-Li alloys Notched bar tensile properties X2020 Ultrasonic Gas Atomization 2024		
20. ABSTRACT (Continue on reverse side if necessary and identify by block number) The literature appears convincing that of the Al-Li alloys, Al-Cu-Li provides stronger alloys than does Al-Mg-Li. Yet, such earlier studies were based on ingot technology where segregation problems could conceivably have worsened actual comparisons. Further, the phase diagrams for these two ternary systems are poorly known, especially if significant additions of Mn, Cd, Cr, Ti, Zr and other elements are made. In fact the Al-Cu-Mg-Li quaternary based on the 2024 alloy gave some rather excellent combinations		

ADA 085354

DTIC ELECTE
S JUN 11 1980 D
B

FILE COPY

DD FORM 1473 1 JAN 73

EDITION OF 1 NOV 65 IS OBSOLETE
S/N 0102-LF-014-6601

Unclassified

SECURITY CLASSIFICATION OF THIS PAGE (When Data Entered)

4109463

TEN TO THE 4TH POWER

TEN TO THE 5TH POWER

of strength and toughness when the alloys were made from rapidly solidified (RS) particulates. Continuing alloy development, structure refinement, and property assessments, based on RS technology, are the basis of this study. Both 2020 and 2024 base alloys are being prepared by RS powder technology (ultrasonic gas atomization with quench rates of 10⁴ to 10⁵ K/s); lithium contents from about 1 to 3 weight percent are being studied at several different ratios of Cu to Li. Phase identification studies are being planned but only preliminary data are available. Mechanical properties (smooth bar tension tests) appear excellent for the Al-Cu-Li alloys, significantly better than for the 2024 base alloy. Notch toughness tests are still a problem even though improvements are being made.

ACCESSION for	
NTIS	White Section <input checked="" type="checkbox"/>
DDC	Buff Section <input type="checkbox"/>
UNANNOUNCED	<input type="checkbox"/>
JUSTIFICATION _____	
BY _____	
DISTRIBUTION/AVAILABILITY CODES	
Dist.	AVAIL. and/or SPECIAL
A	

STRUCTURE AND PROPERTIES OF RAPIDLY SOLIDIFIED

2000 SERIES Al-Li ALLOYS

N. J. Grant, S. Kang and W. Wang
Massachusetts Institute of Technology
Cambridge, Massachusetts

ABSTRACT

The literature appears convincing that of the Al-Li alloys, Al-Cu-Li provides stronger alloys than does Al-Mg-Li. Yet, such earlier studies were based on ingot technology where segregation problems could conceivably have worsened actual comparisons. Further, the phase diagrams for these two ternary systems are poorly known, especially if significant additions of Mn, Cd, Cr, Ti, Zr and other elements are made. In fact the Al-Cu-Mg-Li quaternary based on the 2024 alloy gave some rather excellent combinations of strength and toughness when the alloys were made from rapidly solidified (RS) particulates. Continuing alloy development, structure refinement, and property assessments, based on RS technology, are the basis of this study. Both 2020 and 2024 base alloys are being prepared by RS powder technology (ultrasonic gas atomization with quench rates of 10^4 to 10^5 K/s); lithium contents from about 1 to 3 weight percent are being studied at several different ratios of Cu to Li. Phase identification studies are planned but only preliminary data are available. Mechanical properties (smooth bar tension tests) appear excellent for the Al-Cu-Li alloys, significantly better than for the 2024 base alloy. Notch toughness tests are still a problem even though improvements are being made.

80 6 11 030

Introduction

Extensive efforts are being made to develop high strength-high modulus-low density aluminum alloys for aircraft structural applications, in particular alloys based on the Al-Li system. Sanders and Balmuth (1) recently pointed up the potential of Al-Li alloys in terms of strength and other properties; however, the difficulties in casting and fabricating these alloys, based on the segregation of lithium in slowly solidified cast products, and the resultant low fracture toughness limited the use of these alloys.

Recent developments in rapid solidification (RS) processes have spurred the evolution of high strength aluminum alloys and have shown the potential for achieving high strength, useful ductility, fracture toughness, fatigue resistance, and resistance to stress corrosion cracking through the attainment of highly refined structures (2,3).

In the present study 2XXX series aluminum alloys which contain from 1 to 3% lithium were chosen (X 2020 and 2024) and produced via RS powder metallurgy. The effects of RS powder metallurgy processes on the structure and properties of these alloys will be considered, along with splat quenched 2024 alloy containing lithium.

A. Experimental Procedure

Master alloys were received in ingot form from Reynolds Metals Co. Table 1 lists the chemical compositions of the as-received and the as-extruded RS alloys.

A schematic diagram of the atomization apparatus is given in Fig. 1. To minimize oxidation of the melt, the melting chamber was evacuated and then backfilled with argon to a slight positive pressure. The re-melt ingot was induction melted and superheated to 820°C. Atomization was accomplished using an ultrasonic gas atomization die described elsewhere (4). The impingement angle of the gas jets on the metal stream was 45°. Gas pressures (gage) of 1200 psi were used, resulting in gas velocities indicated to be in the range Mach 2 to 2.5. Detailed discussion and procedures of atomization can be found from references (5-7).

The atomized powders were collected and sieved through 325, 270 and 120 mesh screens (44, 54, and 122 microns) to establish a general distribution of powder particle sizes. Final characterization (i.e., size, shape, dendrite arm spacing) was done using a Cambridge Scanning Electron Microscope.

All of the following fabrication was done at Nuclear Metals, Concord, Mass. The powders were canned in a 6061-T6 aluminum container and cold compacted at 4000 psi accumulator pressure to approximately 80% of theoretical density. The cans were heated to 400°C and evacuated, sealed off and extruded at 400°C at a 30 to 1 extrusion ratio to produce 1-1/2" x 1/2" rectangular bar sections. Excellent extrusions were obtained in all cases.

In order to determine the optimum heat treatments various solution and aging temperatures were tried for various times. Heat treatments were conducted in a non-circulating air furnace and silicon oil bath.

A Cambridge Stereoscan Scanning Microscope was used for studies of the fracture surfaces of tensile and notch-tensile specimens. A Scanning Auger Microscope was used to check the impurity levels on the fracture surfaces of the 2020 P/M alloys. Element mapping was conducted to determine the distribution of impurities.

Room temperature tensile and notch-tensile tests were conducted on an Instron machine. Density and Young's modulus were determined by Archimedes' principle and by an ultrasonic (10 MHz) pulse-super-position method (8), respectively.

B. Results and Discussion

1. Atomization of Alloys

The size distributions of atomized alloys, which are averaged results of 3-4 runs, are shown in Fig. 2. It was a primary goal to produce more or less smooth, spherical particles by ultrasonic gas atomization; however, some variations from smoothness and roundness are usual in aluminum atomization. Figure 3 shows a typical SEM view of atomized powder particles of alloy 2024-72. Most of the powders produced for this study have shown a similar spherical morphology. It seems that the spherical morphology of the powders is strongly dependent upon a uniform delivery of a gas stream (laminar flow) to the metallic stream. Deviations from sphericity occur due to gas turbulence and the presence of stiff refractory oxide films. Figure 4 shows a typical SEM view of dendrites shown on the surface of a 14 μm powder particle of alloy 2024-72.

A plot of dendrite arm spacing (DAS) vs. powder particle size is shown in Fig. 5 for each alloy. Figure 6 shows a plot of DAS vs. solidification rate (9), from which it is estimated that the quench rate for these alloys varied from 10^4 to 10^5 K/s. DAS measurements on polished sections point up the uniformity of cooling rate through the thickness of the powders, an important advantage of RS atomization processing.

2. Consolidation

Microstructures of the as-extruded alloys 2024-72 and 2024-33 are shown in Fig. 7. Alloy 2024-72 was preheated to 500°C mistakenly to decompose hydrate presumed to be present on the powder surfaces. Alloy 2024-32 was heated only to 400°C and extruded at the same temperature. Note the marked coarsening of alloy 2024-72. In both alloys significant precipitation has occurred due to exposure to 400 and 500°C. No hydrogen blistering was observed in any of the argon atomized alloys even on exposure to 535°C for time periods up to one hour.

3. Solution Heat Treatment and Aging Response

Figure 8 shows TEM views of RS 2020-68 alloy taken after solution heat treatment. Note that the fine microstructure of 2-3 μm grain size is maintained after solution treatment. No recrystallization was noticed in any of the alloys. This may be attributed partially to a grain stabilizing effect (Mn in this system), as well as to finely dispersed oxide particles which are distributed more or less uniformly throughout the matrix. There appear to be two phases present in the

Fig. 8 TEM views, probably AlLi and Al₂O₃, however the phases have not yet been identified.

Aging response was determined to try to obtain optimum combinations of strength and fracture toughness. For the RS 2020 alloys the overaged condition was used rather than the underaged to enhance fracture toughness. Cold work followed by solution treatment and aging was also studied for the RS 2020 alloys for the same reason. All heat treatment conditions are listed in Table 2.

4. Properties of Heat Treated Alloys

4.1 Physical Properties

The density and elastic modulus values of each alloy are given in Table 3 along with other values obtained from the literature. The reduced density is a direct result of the presence of lithium and indicates that the lithium is present in the form of intermetallic compounds rather than oxide, and increased elastic modulus values are attributed to the presence of δ' (Al₃Li).

4.2 Tensile Properties

The tensile properties of these alloys are given in Table 4. As can be seen, improved strength with the addition of lithium is achieved in all cases; however, no improvement in elongation is observed except for RS 2020 alloys. Higher strength levels obtained in these alloys are primarily due to co-precipitation of θ'' (Al₂Cu) and δ' (Al₃Li), and secondly, due to the highly refined structures. It is natural that higher strength is obtained with higher lithium content since lithium provides a large volume fraction of δ' structure. It appears that the refined structure of RS 2020 alloys is not sufficient to counteract the inherent fracture mechanism which is associated with the presence of the coherent ordered precipitates of δ' (Al₃Li). However, an optimum combination of refined structure and dispersoid volume and type should provide the basis to minimize this problem in RS 2020-type alloys. One obtains comparable values of elongation to that of ingot 7075-T6 in RS 2020-68 through cold work before solution treatment. Further there is no loss of strength in the cold worked RS 2020-68 alloy compared to the peak aged RS 2020-68-T6 alloy. This may be attributed in part to a more uniform distribution of fine oxide particles throughout the matrix as a result of the cold work. These incoherent oxide particles are effective as dispersoids which make slip less localized, resulting in higher ductility. Furthermore, it seems that a portion of the cold work is retained even after solution treatment, and provides higher strength than the T6 temperature. RS 2020-69 alloy did not respond in the same way; however this alloy had a somewhat different pretreatment (see Table 2) than RS 2020-68. Further investigation is in progress with these alloys. Figures 9 and 10 show fracture surfaces of these alloys. Since the RS alloys have a very small grain (2-3 μ m), as shown in Fig. 8, it is hard to distinguish intergranular failures from transgranular; however, the small dimples observed on the fracture surfaces of Fig. 9 suggest that a mixed mode of inter- and transgranular fractures prevails (for unknown reasons) in Al-Li alloys produced by rapid solidification processes.

Generally, RS 2020 alloys show higher strength values than RS 2024 alloys containing lithium. The presence of Mg in 2020 alloy limits the

solution temperature to less than 500°C thereby limiting the solubility of Cu to about 4 wt %. The higher solution treatment temperature of 525°C for RS 2020 permits dissolution of additional amounts of Cu, which is ultimately available for precipitation (10). The presence of Cd in the RS 2020 alloy is presumed to modify the aging behavior and thus may provide additional strength.

4.3 Notch Tensile Properties

Kaufman and Johnson (11) showed that the notch-yield ratio (ratio of notch tensile strength to smooth bar tensile yield strength) is a more useful criterion for rating relative notch sensitivities than is the notch-strength ratio (ratio of notch tensile strength to smooth bar tensile strength) in aluminum alloys. According to this criterion, in general, the ingot product alloys X2020-T6, 2024-T86 and 7075-T6 are found in the lowest range among other aluminum alloys. X2020-T6 is the worst of the group (12). Table 4 shows the details of such notched tests, from which it is clear that these Al-Li alloys do not show a notch-strengthening effect.

Impurity levels of the RS 2020 alloys were checked using a Scanning Auger Microscope. It has been suggested that sodium, which is a major impurity in lithium alloyed materials, is responsible for the embrittlement in aluminum. It is also known that the presence of potassium and sulphur, which normally segregate at grain boundaries, may account for intergranular failure. No impurity was found other than sulphur in alloy 2020-68. Webster (13) has shown that neither the levels of sodium nor potassium correlate with the observed toughness or ductility regardless of whether the alloy contains lithium. Similar conclusions might be drawn from the data shown here since alloy 2020-69, which does not have any impurities on its fracture surfaces, shows lower ductility than RS alloy 2020-68, which has sulphur as an impurity. Fig. 11 (a) and (b) show the distribution of sulphur on the fracture surface of RS alloy 2020-68, clearly showing areas of heavy sulfur concentration.

RS 2024-Li PM Alloys

Considerably less work has been done thus far with the RS 2024-Li PM alloys, and only a preliminary appraisal is given here. The strength values are not quite as good as those of Sankaran and Grant (10) but the ductilities for a given lithium content appear to be a little better.

One of the two RS 2024-Li alloys was incorrectly processed prior to extrusion. RS alloy 2024-72-T4, containing 1.29% Li (Table 1B) was held at 500°C for at least one hour prior to extrusion at 400°C. Figure 7a shows the resultant coarse structure of the alloy compared to RS 2024-32-T6, which was subjected to a normal degassing treatment of 400°C (Fig. 7b). Tension properties of the RS 2024-72-T4 alloy are correspondingly poor (Table 4).

A further complication is that the RS 2024-72 alloy has the unusually high copper content of 5.92, which leads to the presence of a relatively coarse CuMgAl₂ phase after the double exposure of the alloy to about 500°C. Figure 11a shows the brittle fracture of these coarse inter-

metallics. Figure 11b identifies the fractured brittle phases to be copper-rich.

Acknowledgements

The authors are pleased to acknowledge the support of this study by DARPA under contract N00014-78-C-0385.

References

1. T. H. Sanders and E. S. Balmuth: Metal. Prog. March 1978, p. 33.
2. J. P. Lyle and W. S. Cebulak: Met. Trans A. Vol 6A, 1975, p. 685.
3. W. S. Cebulak, E. W. Johnson and H. Markus: Int. J. of Powder Met. Vol. 12, No. 4., 1976, p. 299.
4. J. Hartman: J., Phil. Mag., 11 (1931), p. 926.
5. A. Lawley: Int'l. J. of Powder Metall. & Powder Tech. Vol. 13, No. 3, July 1977, p. 169.
6. N. J. Grant: Rapid Solidification Processing: Principles and Technologies. Proc. Int'l Conf. on RSP, Virginia, Cohen, Kear, Mehrabian, Eds., Claitor's Publishing Div., Nov. 1977, p. 230.
7. V. Anand: "A High Strength P/M Al-Zn-Mg-Cu-Fe-Ni Alloy Using Ultrasonic Atomization" S.M. Thesis, MIT, Cambridge, Mass., August 1977.
8. E. R. Naimon, H. M. Ledbetter and W. F. Weston: J. Mat. Sci., Vol. 10, 1975, p. 1309.
9. H. Matyja, B. C. Giessen and N. J. Grant: J. Inst. Metals, Vol. 96, 1968, p. 30.
10. K. K. Sankaran and N. J. Grant: Structure and Properties of Splat Quenched 2024-type Al Alloy containing Li, Accepted for publication Jour. Mats. Sci and Eng., 1980.
11. J. G. Kaufman and E. W. Johnson: Proceedings, ASTEA, Am. Soc. Testing Mats., Vol. 62, 1962, p. 778-793.
12. E. H. Spuhler: A. H. Knoll and J. G. Kaufman: Metal Prog., Vol. 79, 1960, p. 80.
13. D. Webster: Met. Trans. A., Vol. 10A, December, 1979, p. 1913.

Table 1A. Chemical Compositions of As-Received Al Alloys

	<u>Cu</u>	<u>Mg</u>	<u>Li</u>	<u>Mn</u>	<u>Cd</u>	<u>Fe</u>	<u>Si</u>	<u>Zn</u>	<u>Al</u>
RS 2020-68	4.61	0.01	1.42	0.5	0.21	0.10	0.04	0.02	bal
RS 2020-69	4.32	0.01	1.88	0.5	0.22	0.11	0.04	0.02	bal
RS 2024-72	5.65	1.50	1.58	0.48	0.20	0.11	0.05	0.02	bal
RS 2024-32	3.96	1.57	2.17	—	—	0.10	0.05	0.02	bal

Table 1B. Compositions of As-Extruded Al Alloys

	<u>Cu</u>	<u>Mg</u>	<u>Li</u>	<u>Mn</u>	<u>Cd</u>	<u>Fe</u>	<u>Si</u>	<u>Zn</u>	<u>Al</u>
RS 2020-68	4.61	0.013	1.04	0.39	0.11	0.22	0.06	0.015	bal
RS 2020-69	4.32	0.031	1.52	0.38	0.15	0.17	0.06	0.013	bal
RS 2024-72	5.92	1.57	1.29	0.36	0.13	0.18	0.06	0.013	bal
Splat 2024 + 1% Li (Alloy A)	4.1	1.3	1.0	0.6	—	0.5	< 0.06	< 0.02	bal
Splat 2024 + 3% Li (Alloy B)	3.4	1.1	3.2	0.6	—	0.4	< 0.06	< 0.02	bal

Table 2. Processing and Heat Treatments of Alloys

<u>Alloy and Temperature</u>	<u>Preparation for Extrusion*</u>	<u>Heat Treatments**</u>
2020-68-T6	500°C degassing for 1 h	S.T. 525°C, 1 h + age 175°C, 16 h
2020-68-T7	500°C degassing for 1 h	S.T. 525°C, 1 h + age 175°C, 16 h + 190°C, 4 h
2020-69-T6	400°C preheat	S.T. 525°C, 1 h + age 175°C, 14 h
2020-69-T7	400°C preheat	S.T. 525°C, 1 h + age 175°C, 14 h + 190°C, 4 h
2024 + 1% Li - T4 ⁽¹⁾	400°C preheat	S.T. 495°C, 1 h + age 20°C, 7 days
2024 + 1% Li - T6 ⁽¹⁾	400°C preheat	S.T. 495°C, 1 h + age 190°C, 12 h
2024 + 3% Li - T6 ⁽²⁾	400°C preheat	S.T. 495°C, 1 h + age 165°C, 12 h
2024-72-T4	500°C degassing for 1 h	S.T. 495°C, 1 h + age 20°C, 23 days
2024-72-T6	500°C degassing for 1 h	S.T. 510°C, 1 h + age 190°C, 9 h
2024-32-T4	400°C preheat	S.T. 495°C, 1 h + age 20°C, 12 days

* Accumulator pressure 4000 psi; 1 h at temp; extrusion ratio 30:1; bar size cross section 1.5 x 0.5 in.

(1) Sankaran alloy A

(2) Sankaran alloy B

** Cold water quench from solution temperature

Table 3. Physical Properties of Aluminum Alloys

<u>Alloy</u>	<u>Wgt % Li</u>	<u>Modulus (psi x 10⁶)</u>	<u>Density (g/cm³)</u>
pure Al	-	9.0	2.699
2020-68-T6	1.0	11.3	2.677
2020-69-T7	1.5	11.4	2.623
2024-T4	-	10.6	2.768
Alloy A (10) (2024 + 1 wgt % Li)	1.0	11.2	2.685
Alloy B (10) (2024 + 3 wgt % Li)	3.2	12.3	2.519
7075-T6	-	10.4	2.796
2024-72	1.3	-	2.700
2024-32	2.2	-	2.620

Table 4. Tensile Properties

<u>Alloy and Temperature</u>	<u>wt% Li</u>	<u>0.2% YS (KSI)</u>	<u>UTS (KSI)</u>	<u>Elong. (%)</u>	<u>RA (%)</u>
Ingot 2020-(T6)	1.3	77.0	84.0	3.0	-
RS 2020-68-(T6)	1.0	81.9	87.9	5.8	8.9
RS 2020-68 (C.W.*+T6)	1.0	82.2	89.4	8.9	14.7
RS 2020-69 (T7)	1.5	90.4	94.3	5.3	6.3
RS 2020-69 (C.W.*+T7)	1.5	80.3	84.8	5.3	6.0
<hr/>					
Ingot 2024-(T4)	-	41.5	64.1	23.8	23.5
RS 2024-72(T4)	1.3	40.5	57.2	20.0	15.4
RS 2024-72 (H.R.**+T4)	1.3	47.7	64.5	10.8	9.7
RS 2024-72(T6)	1.3	60.0	67.5	10.0	7.3
RS 2024-32(T6)	2.2	55.4	70.4	8.0	8.0
<hr/>					
Splat Alloy A(T4) [†] (2024 + Li)	1.0	56.3	76.0	20.7	9.2
Splat Alloy A(T6) [†]	1.0	63.5	77.5	8.2	5.2
Splat Alloy B(T6) [†]	3.0	82.8	84.5	5.1	2.5

C.W.* - cold swaged to 45% RA before solution treatment

H.R.** - hot rolled (400°C), 56% thickness reduction

† Sankaran and Grant data (reference 10)

Table 5. Notch Tensile Properties of RS Alloys

<u>Alloy and Temper</u>	<u>Elong (%)</u>	<u>RA (%)</u>	<u>NTS ** (ksi)</u>	<u>UTS (ksi)</u>	<u>YS (ksi)</u>	<u>σ_{NTS}/σ_{YS}</u>
2020-68 T6	5.8	8.9	65.3	87.9	81.9	0.80
2020-68 T7	6.3	15.5	66.1	80.6	74.5	0.89
2020-68 (S.T. + aged at 175°C for 40 hrs)	5.5	10.2	73.4	82.2	76.6	0.96
2020-68 (C.W.* + T6)	8.9	14.7	60.2	89.4	82.2	0.73
2020-68 (C.W.* + T7)	10.8	16.0	64.9	85.4	78.4	0.83
2020-69 T7	5.3	6.0	42.8	94.3	90.4	0.47

C.W.* = swaged 40% reduction of area; proportional dimensions were used, maintaining the ratio of notch radius to major radius because of size limit after swaging

NTS** = all values are results of one test except 2020-68 T6 and 2020-69 T7 (average of two tests)

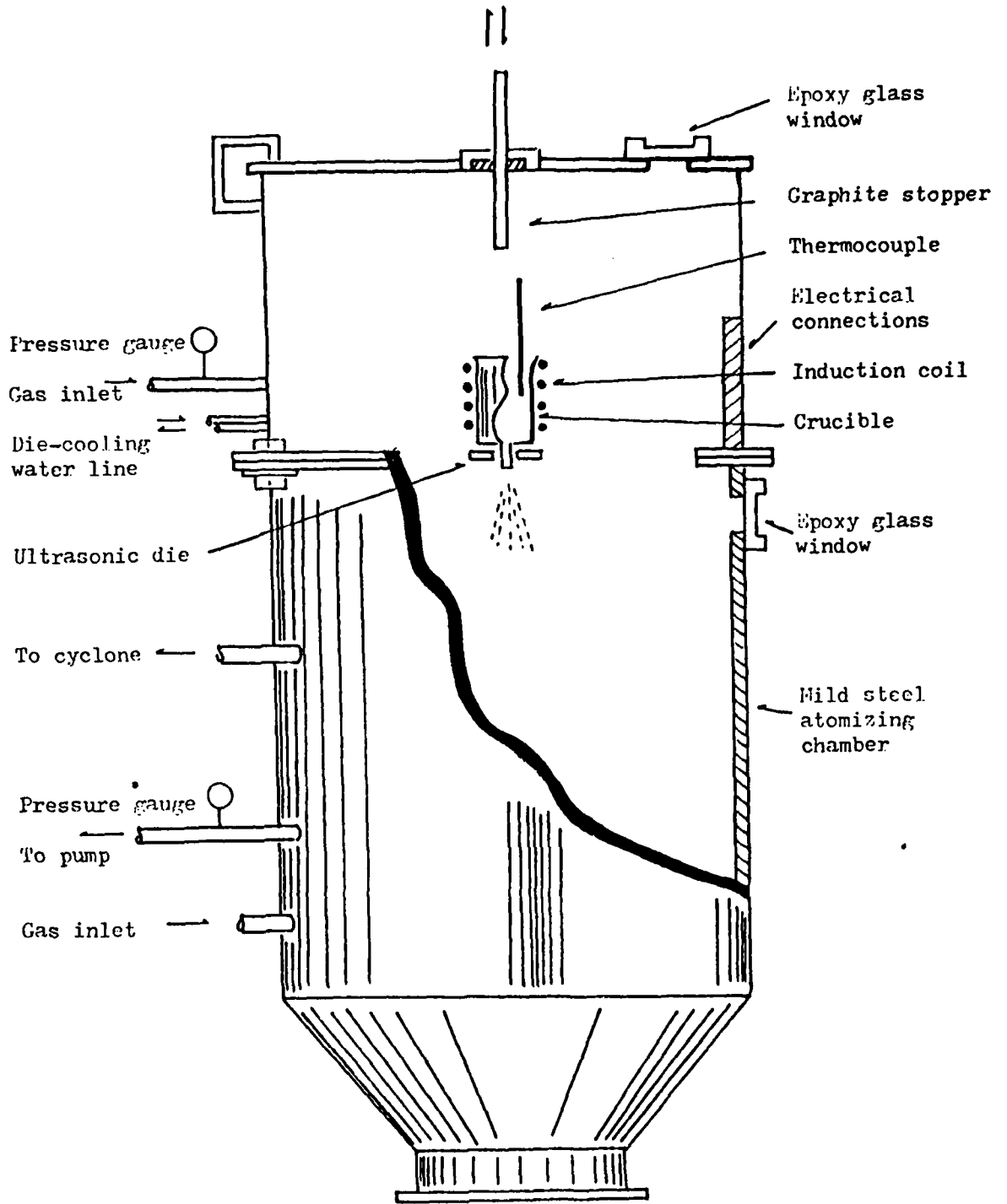
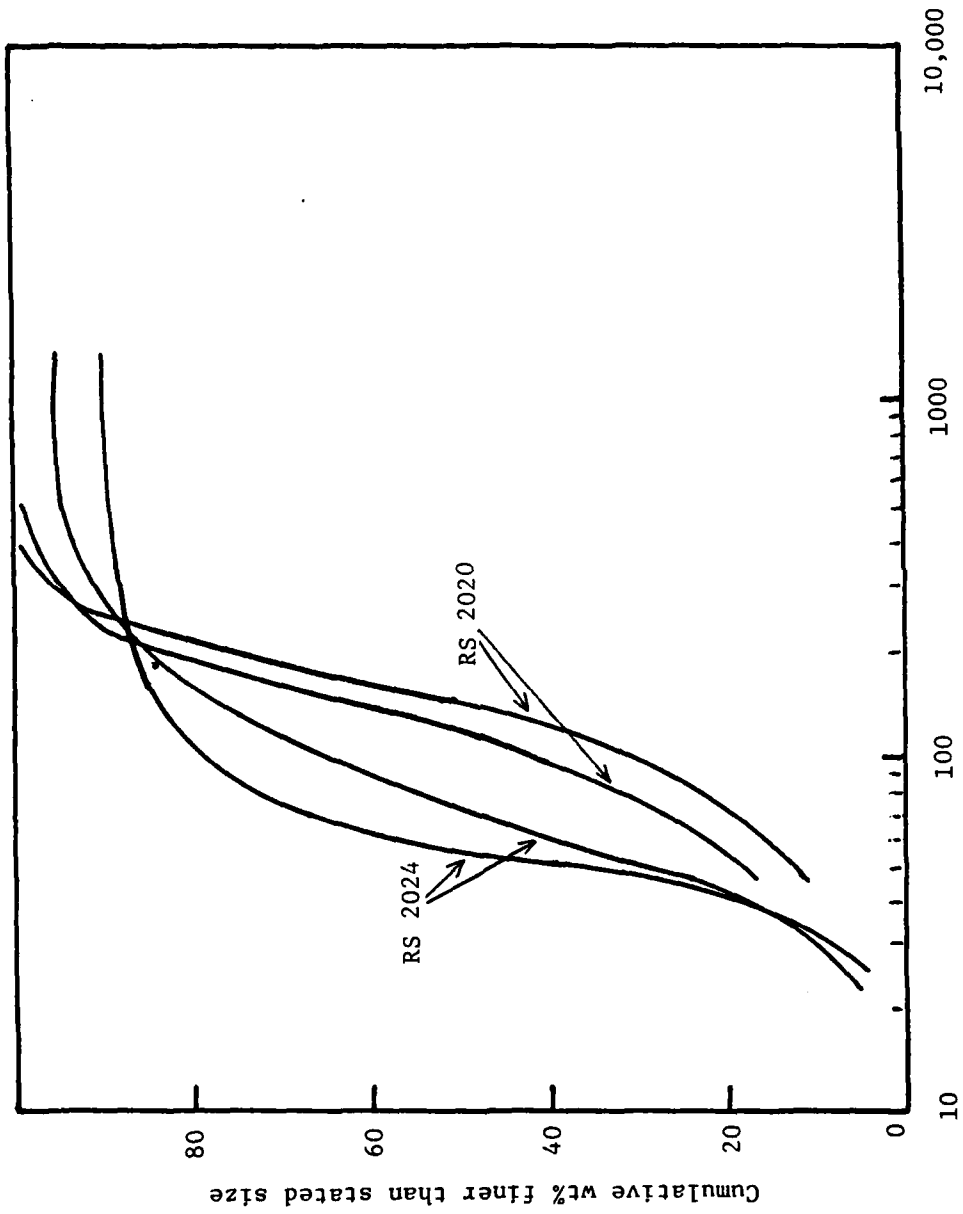


Fig. 1: Schematic Diagram of the Atomizing Unit



Powder size, microns

Figure 2. Screen analyses of USCA aluminum powders

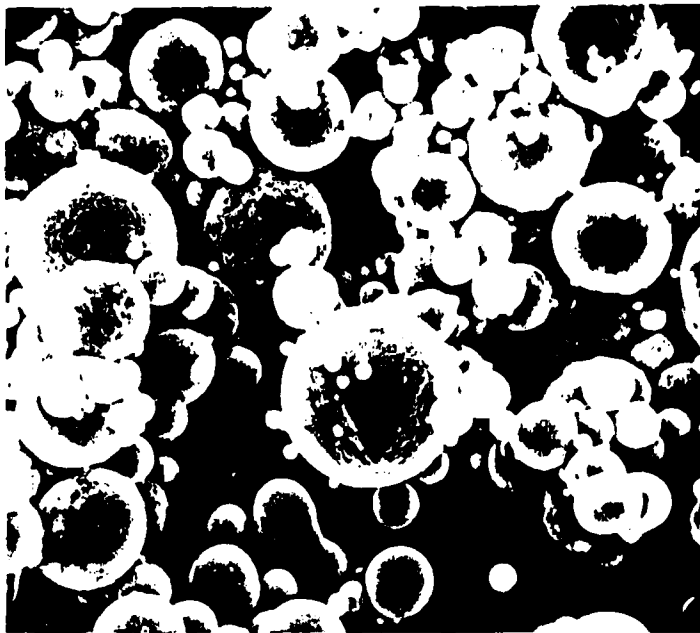


Figure 3. SEM micrograph for ultrasonically atomized powders: alloy 2024-72. 1000 X



Figure 4. A typical ultrasonically atomized powder particle. Alloy 2024-72. 6000 X

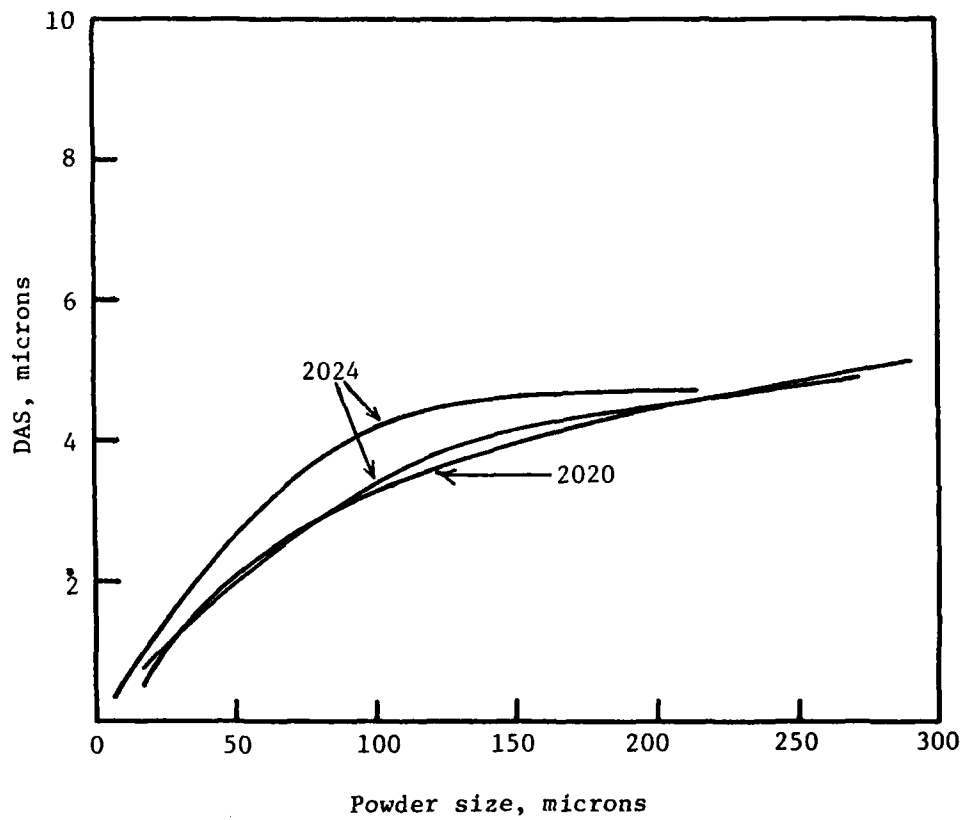


Figure 5. Dendrite arm spacing as a function of powder size for 2020 and 2024 RS aluminum alloys.

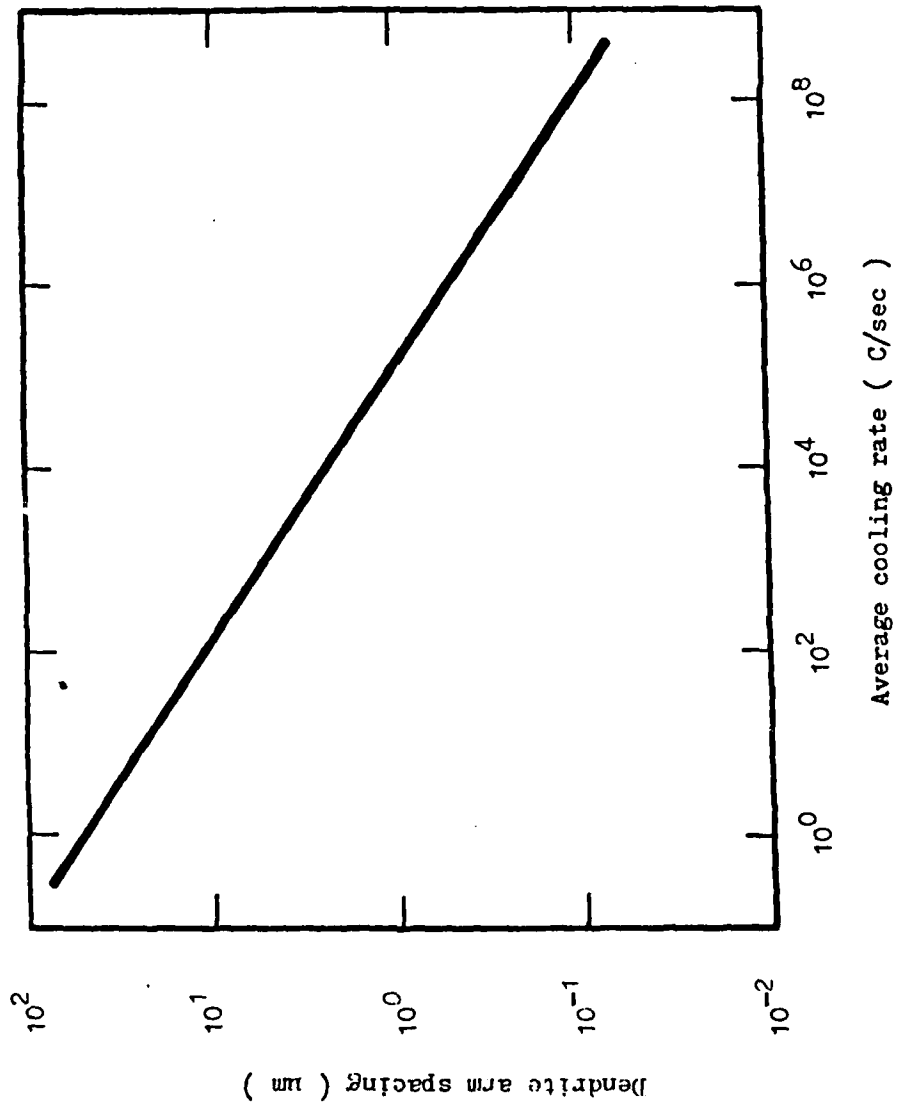


Fig. 6. Variation of the Dendrite Arm Spacing with Cooling Rate for Al Alloys

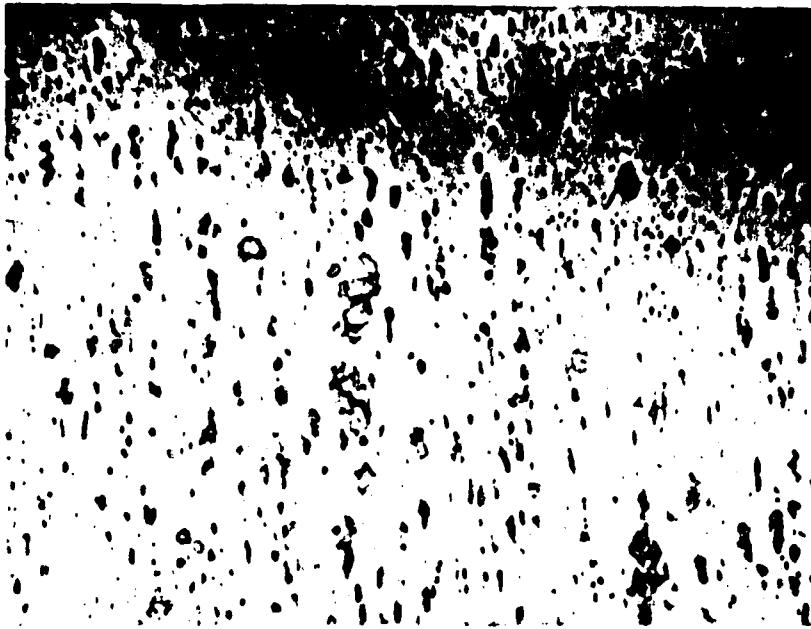


Figure 7a. Microstructure of alloy 2020-72,
preheated to 500°C and extruded at 400°C.
Longitudinal section: 500 X

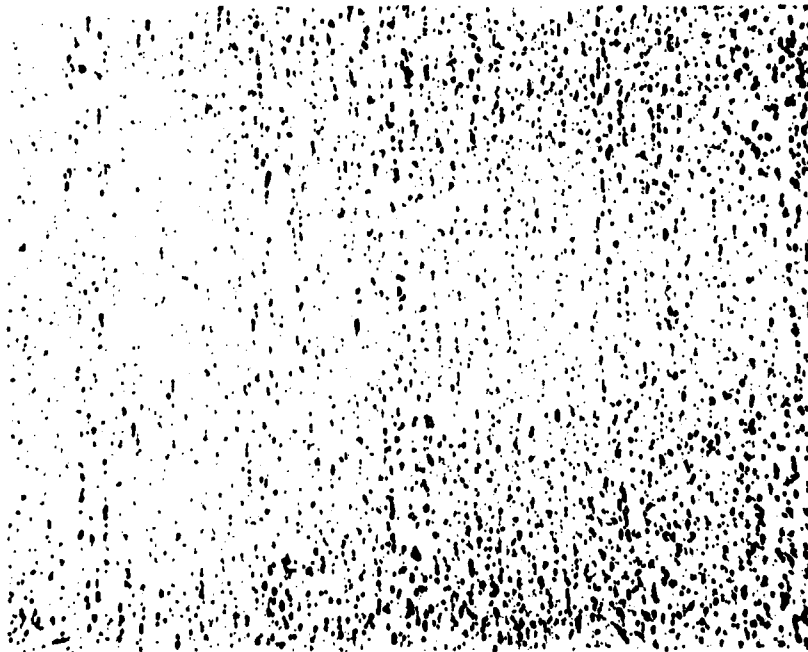


Figure 7b. Microstructure of alloy 2024-32, preheated
and extruded at 400°C. Longitudinal
section: 500 X

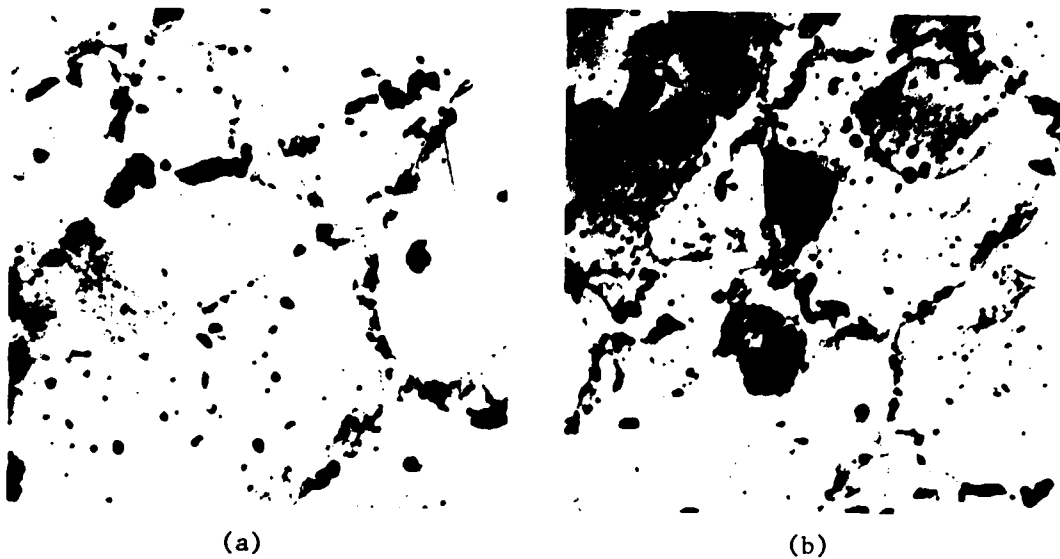


Figure 8. TEM micrographs of RS 2020-68 alloy after solution treatment at 525°C for 1 hr.
a) 9400 X b) 6000 X.
Grain size 2-3 microns

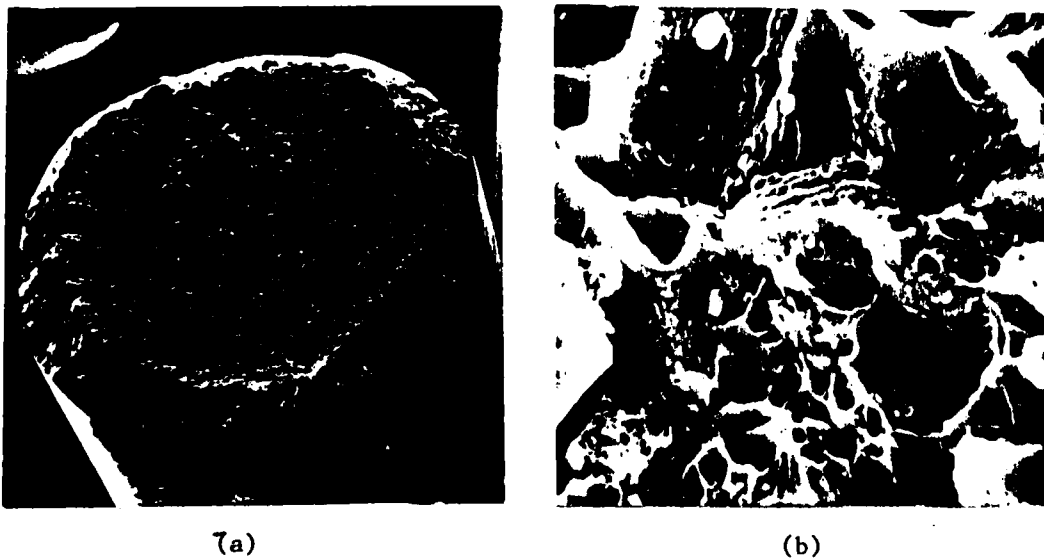


Figure 9. Fracture surfaces of RS 2020-68-T6.
a) 20 X, typical, b) 5000 X, dimples

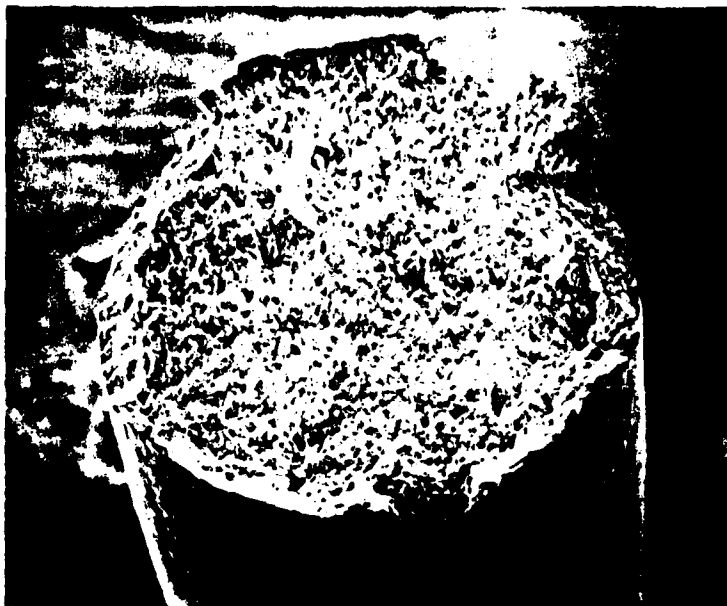


Figure 10. Fracture surface of RS 2020-68 alloy after 45% cold reduction plus 525°C solution treatment plus aging at 175°C, 16 hr. Compare fracture with Figure 9a. 20 X



Figure 11a. Fracture surface of 2020-68
taken from Auger X 500.

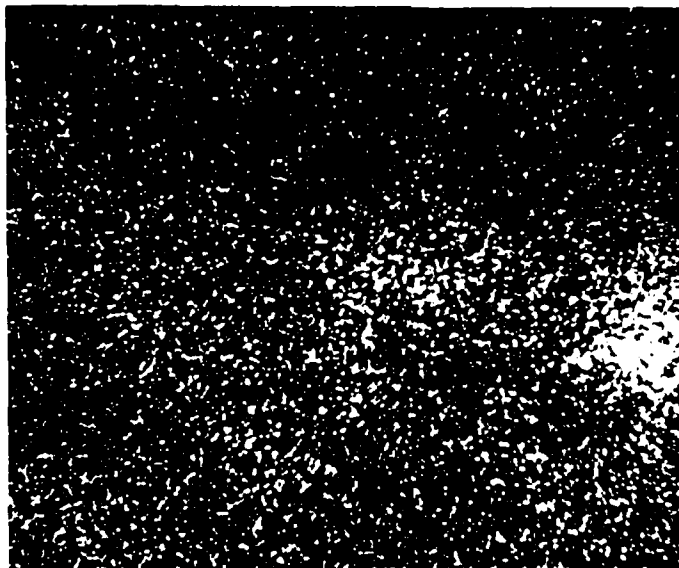


Figure 11b. Distribution of sulphur on the
surface.

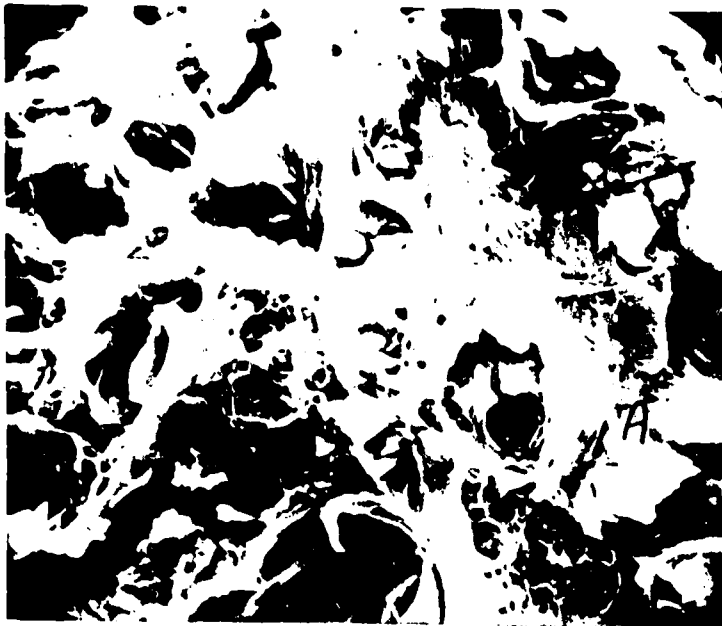


Figure 12a. Tensile fracture surface of alloy 2024-72-T4. 2400 X

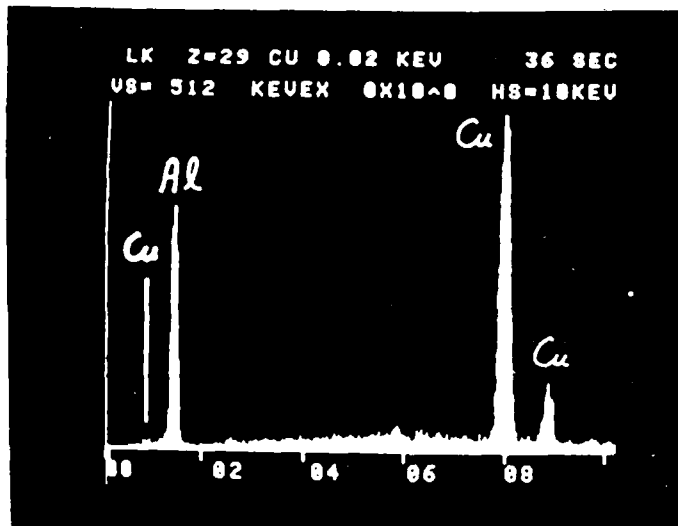


Figure 12b. EDAX on particle A in Figure 12a.